

Short Communication

## Nanostructured Manganese oxide Films for High performance Supercapacitors

Hua Fang<sup>1,\*</sup>, Linsen Zhang<sup>1</sup>, Yalan Xing<sup>2</sup>, Shichao Zhang<sup>2</sup>, Shide Wu<sup>1,\*</sup>

<sup>1</sup> School of Material and Chemical Engineering, Henan Provincial Key Laboratory of Surface Interface Science, Zhengzhou University of Light Industry, Zhengzhou 450001, PR China

<sup>2</sup> School of Materials Science and Engineering, Beihang University, Beijing, 100191, PR China

\* E-mail: [fh@zzuli.edu.cn](mailto:fh@zzuli.edu.cn), [wushide@zzuli.edu.cn](mailto:wushide@zzuli.edu.cn)

Received: 31 April 2018 / Accepted: 28 June 2018 / Published: 5 August 2018

---

Nanostructured manganese oxide films, including continuous coating, nanoflower film and nanowall array, were electrodeposited on nickel foils via anodic electrodeposition. The as-prepared samples were tested as electrodes for supercapacitors and excellent capacitive performances were achieved. Among them, the nanowall array, which was composed of interconnected ultrathin nanosheets, exhibited the highest specific capacitance of 327 F g<sup>-1</sup> at 1 A g<sup>-1</sup>. The specific capacitance could retain as high as 317 F g<sup>-1</sup> after 1000 cycles. The superior capacitance performance can be attributed to its unique nanoporous structure which facilitates fast ion transportation.

---

**Keywords:** Manganese oxide; Supercapacitors; Electrodeposition; Nanostructure; Nanowall

### 1. INTRODUCTION

Electrochemical supercapacitors have gained growing interest due to their high power density, high energy density and excellent long cycle life stability [1-3]. To develop high performance supercapacitors, recent researches have focused on low fabrication cost, high energy density and environmentally benign materials [4-7]. Manganese oxides in various forms have been extensively studied as electrode materials for supercapacitors, owing to their high energy density, abundance of raw materials, and environmental friendly feature [8-15]. However, the performance of Manganese oxides as pseudocapacitor material is hindered by their poor electrical conductivity and mechanical instability [16].

Three-dimensional (3D) mesoporous materials with ordered/apperiodic architectures have drawn

much concern, which facilitate the fast electrolyte ion migration, fast faradic redox reactions and thus improved performances [17-21]. Manganese oxide arrays composed of vertically aligned nanotubes/nanowires have been fabricated by using anodic aluminum oxide (AAO) templates, showing superior capacitive performances [22-27]. Mesoporous manganese oxide films have also been reported and improved capacitive performances were achieved [28-33]. However, the relatively high fabrication cost of the template methods and the environmentally unfriendly nature of the template removal process are two major obstacles to their commercial application. Thus, designing and fabricating nanostructured manganese oxide electrode with high electrochemical performance is still a tremendous challenge [20].

Electrodeposition technique is a low cost and very efficient way to fabricate nanostructured manganese oxide films on conductive substrates. Recently, a series of manganese oxide nanostructures, including continuous coatings, nanorod/nanowall/nanoflower arrays and interconnected nanosheets, have been successfully fabricated via the electrodeposition technique [11, 12, 14, 33-37]. However, the specific capacitances obtained from these manganese oxide nanostructures are relatively low. Therefore, further research is needed to develop novel manganese oxide with ordered/a-periodic microstructure and superior capacitive performance.

In the present work, a series of nanostructured manganese oxide films, including continuous coating, nanoflower and nanowall array, were electrodeposited on commercial nickel foils by anodic constant voltage electrodeposition by varying the  $\text{MnSO}_4$  concentration of the electrolyte and the voltage for deposition. The as-prepared nanostructured manganese oxide films are binder free with strong adhesion between the active materials and the current collectors [14]. The nanoporous microstructure can ensure fast ions transportation and thus superior capacitive performances [17, 18]. The electrochemical capacitive performances of nanostructured manganese oxide films were carefully examined. Test results show that, among the various nanostructured manganese oxide films, the nanowall array exhibit superior capacitive behavior, proving to be a promising electrode material for supercapacitors.

## 2. EXPERIMENTAL

### 2.1 Electrodeposition of manganese oxide films

Nanostructured manganese oxide films, including continuous coating, nanoflower film and nanowall array, were electrodeposited on commercial nickel foils by anodic constant voltage electrodeposition. The potentiostatic electrodeposition experiments were carried out on a Parastat 2273 Analyzer (Princeton Applied Research Corporation) using a three-electrode system. The nickel foil, a Pt plate electrode and a saturated calomel electrode (SCE) were used as working electrode, counter electrode and reference electrode, respectively. The nickel foil (0.01 cm thick) was cut into rectangles (10 mm  $\times$  15 mm), degreased with acetone in an ultrasonic bath, rinsed with pure water and dried at room temperature. Constant voltage of 0.5 or 0.6 V (vs. SCE) was applied for the anodizing process. Aqueous solutions containing manganese (II) sulfate ( $\text{MnSO}_4$ , 0.1 or 0.01 M) and sodium acetate (NaAC, 0.2 M) were used as the plating solution. All the reagents were analytic reagent (AR) and used

as received. The resulted manganese oxide films were rinsed gently with deionized water and then dried in an oven at 200 °C for 2 h. The mass load of the manganese oxide ranged from 0.1 to 0.2 mg cm<sup>-2</sup>.

## 2.2 Materials Characterization

The morphologies and microstructures of the as-prepared manganese oxide films were investigated by field emission scanning electron microscope (FESEM, Hitachi, S-4800) and transmission electron microscopy (TEM, JEOL JEM 2100F). Oxidation state and composition of the manganese oxide films were characterized X-ray photoelectron spectroscopy (XPS) using an AXIS Ultra instrument from Kratos Analytical.

## 2.3 Electrochemical Characterization

Electrochemical measurements were carried out in 0.1 M Na<sub>2</sub>SO<sub>4</sub> aqueous solution by using a three-electrode system. The as prepared nanostructured manganese oxide film, a Pt plate electrode and a SCE were used as working electrode, counter electrode and reference electrode, respectively. Cyclic voltammetry (CV) scans were carried out from 0 to 1.0 V (vs. SCE) at a scan rate of 10 mV s<sup>-1</sup> using a ZAHNER IM6e electrochemical workstation. Galvanostatic charge/discharge (GCD) tests were performed by using a MSTAT8 battery test system (Arbin Instruments). The current densities for the GCD tests ranged from 1 A g<sup>-1</sup> to 15 A g<sup>-1</sup> and the potential range was 0–1.0 V (vs. SCE).

# 3. RESULTS AND DISCUSSION

## 3.1 Materials Characterization

The surface morphologies of the manganese oxide films were successfully tuned by varying the applied anodic deposition voltage and the concentration of the MnSO<sub>4</sub> in the deposition electrolyte. Fig.1 illustrates morphology evolution process from continuous coating to nanoflower film and finally to nanowall array. As shown in Fig. 1a and b, with a deposition voltage of 0.6 V and a plating electrolyte containing 0.1 M MnSO<sub>4</sub> and 0.2 M NaAC, the obtained manganese oxide film is continuous coating composed of numerous short nanofibers. As the deposition voltage is decreased to 0.5 V while maintaining the deposition electrolyte unchanged, the more nanoporous film is obtained with nanoflower morphology. As shown in Fig. 1c and d, the flower shaped film is homogeneous and each oxide nanoflower is composed of 4-6 petals which are very thin oxide nanosheets.

As the concentration of the MnSO<sub>4</sub> was reduced to 0.01 M, the nanowall array is achieved with the low deposition potential of 0.5 V. As shown in Fig. 1e and f, the oxide nanowalls are randomly oriented composed of ultrathin interconnected oxide nanosheets. The microstructure of the oxide nanowall array can be depicted by the schematic representation shown in the inset of Fig. 1f. The nanowalls, composed of interconnected nanosheets, are vertically aligned on the metal substrate in a

haphazard manner to form a 3D nanoporous film. The aperiodic nanoporous microstructure can ensure appropriate wetting of the electrolyte and provide short diffusion path for electrolyte ions through the whole thickness of the oxide film electrode, leading to fast ions transportation and superior capacitive performances [17, 18].

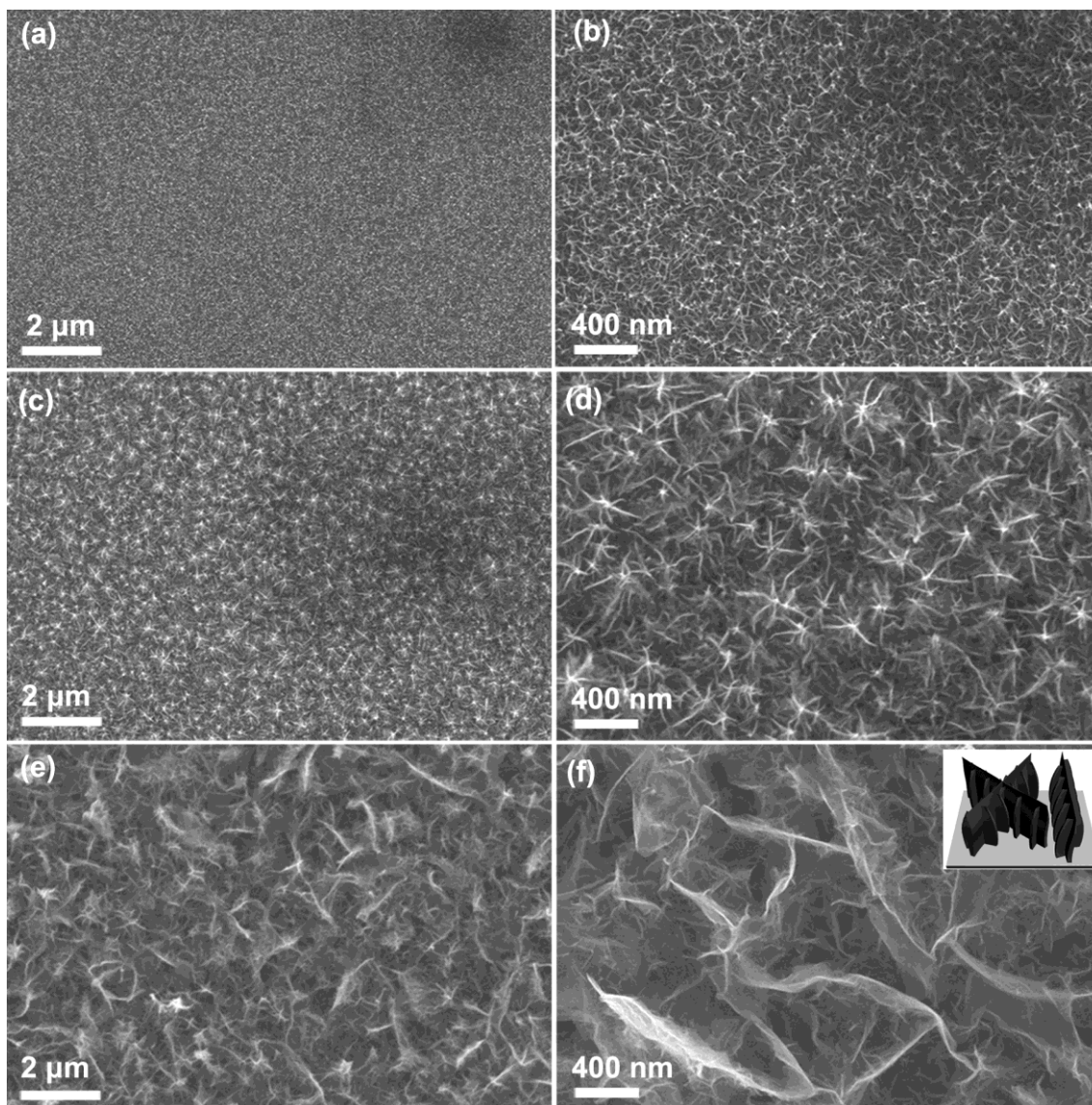


**Figure 1.** SEM images of the nanostructured manganese oxide films: (a) and (b) continuous coating prepared from 0.1 M  $\text{MnSO}_4$  + 0.2 M NaAC solution at deposition voltage of 0.6 V (vs. SCE); (c) and (d) nanoflower film obtained from 0.1 M  $\text{MnSO}_4$  + 0.2 M NaAC solution at deposition voltage of 0.5 V (vs. SCE); (e) and (f) nanowall array prepared from 0.01 M  $\text{MnSO}_4$  + 0.2 M NaAC solution at deposition voltage of 0.5 V (vs. SCE); and inset of (f) schematic representation of the nanowall array.

TEM and selected area electron diffraction (SAED) were performed to understand the microstructure of the nanowalls in further detail. As shown in Fig. 2a, the manganese oxide nanowall array exhibits wrinkled morphology similar to chemically reduced graphene oxide sheets,

demonstrating that the nanowall is composed of ultrathin nanosheets. As shown in Fig. 2b, the fibrous feature is the lateral view of the nanosheets, indicating that the nanosheets are only 2-5 nm thick. As shown in the inset of Fig. 2b, the rings in the SAED pattern of the manganese oxide nanowall array are consistent with the previous reports, demonstrating the antifluorite-type structure [34,36,38].

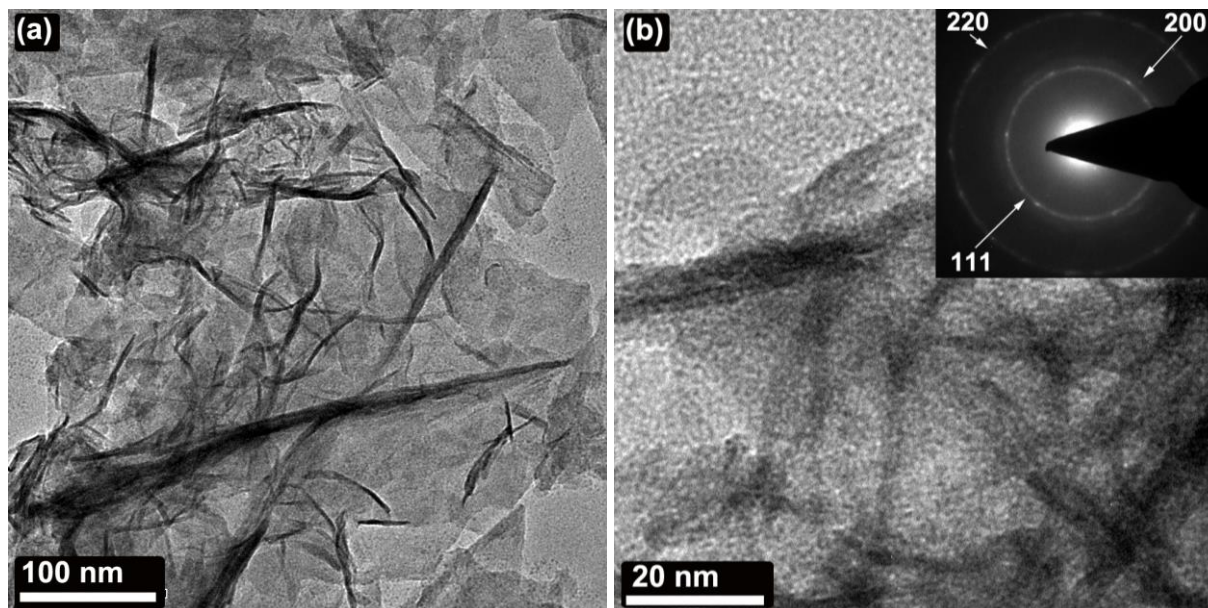


**Figure 2.** Representative TEM images (a and b) and the SAED spectrum (inset of Fig. 2b) of the nanowall array.

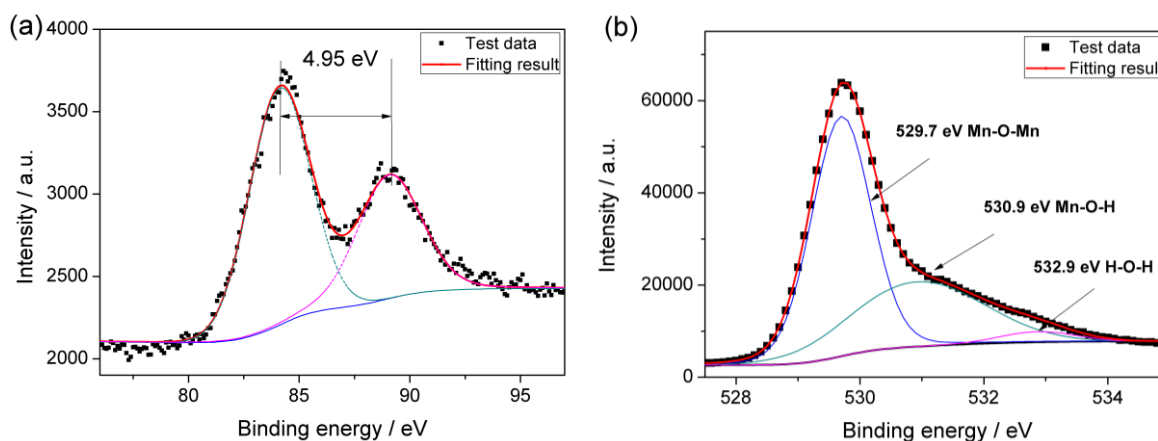


**Figure 3.** XPS spectra from the nanowall array: (a) Mn 3s, and (b) O 1s.

The nanostructured manganese oxide films were subjected to XPS analysis to determine their chemical information. All the samples generate essentially similar XPS spectra. The representative Mn 3s and O 1s spectra from the nanowall array are shown in Fig. 3. As shown in Fig. 3a, the Mn 3s spectra splits into a doublet of peaks due to the parallel spin coupling between the 3s electron and the 3d electron during the photoelectron ejection. The splitting width ( $\Delta E$ ) is reported to have a good linear relationship with the Mn oxidation state ( $n$ ,  $2 \leq n \leq 4$ ) following the equation of  $\Delta E \approx 7.88 - 0.85n$  [39].

Based on the experimental splitting width in the Mn 3s spectra ( $\Delta E = 4.95$  eV, as shown in Fig 3a), the oxidation states of manganese is calculated to be +3.5. As shown in Fig. 3b, the O 1s spectra can be deconvoluted into three different types of oxygen bonds: Mn-O-Mn near 529.7 eV, Mn-O-H near 530.9 eV, and H-O-H near 532.9 eV [40]. The above mentioned XPS results are in good accordance with the previous studies and the as-deposited manganese oxides can be determined as a mixture of manganese dioxide and manganese oxyhydroxide [34].

### 3.2 Electrochemical Characterization

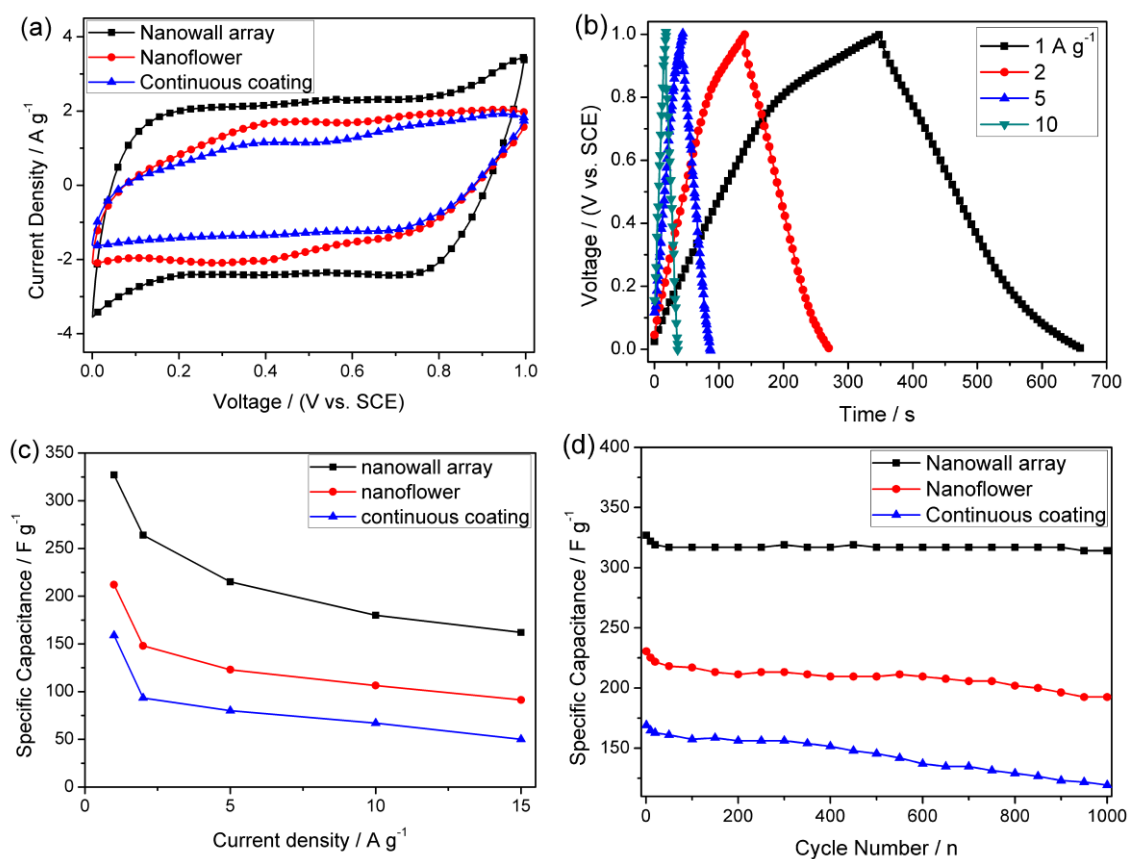


**Figure 4.** Capacitive performances of the nanostructured manganese oxide films: (a) CV curves at 10 mV s<sup>-1</sup>; (b) GCD curves from the nanowall array; (c) rate performance; (d) cycle performance.

To examine the electrochemical properties of the nanostructured manganese oxide films, CVs were carried out in 0.1 M Na<sub>2</sub>SO<sub>4</sub> at a scan rate of 10 mV s<sup>-1</sup>. As showed in Fig. 4a, all the CV curves are close to rectangular shapes, indicating their ~~ideal capacitive behavior~~ excellent pseudocapacitive behavior and low contact resistance [14, 32, 34]. Such excellent capacitive behavior could be attributed to the nanostructures of the electrodeposited manganese oxide films, which can facilitate fast ion transport and provide more electroactive sites [14,32]. The nanowall array provides the most ideal rectangular shaped CV curve with the largest response current, demonstrating its best capacitive performance. The nanowall array film is composed of interconnected nanosheets and has a 3D

nanoporous structure. Such nanoporous manganese oxide films can provide a large active surface area and more electrolyte ions accessible active sites, leading to a high utilization of active materials and thus high specific capacitance [32, 36, 37].

GCD tests were also used to examine the electrochemical properties of the manganese oxide nanostructures. As shown in Fig. 4b, the GCD curves of the manganese oxide nanowall array exhibit ideal triangular shapes under all the GCD current densities, which is the characteristic of ideal capacitive behavior. The specific capacitance (SC) of the manganese oxide nanostructures was calculated from the GCD discharge curves based on the equation of  $SC = (I \Delta t) / (m \Delta U)$ , where  $I$  is the discharge current (in amperes),  $m$  is the mass of manganese oxide loaded on the electrode (in grams) and  $\Delta t$  is the time period (in seconds) for  $\Delta U$  (the voltage change, in volts), respectively [41]. As shown in Fig. 4c, the SC of the nanowall array reaches the highest value of  $327 \text{ F g}^{-1}$  at low current density of  $1 \text{ A g}^{-1}$ , and declines gradually along with the increase of the GCD current density. The SC decreases to  $162 \text{ F g}^{-1}$  as the current density increased to  $15 \text{ A g}^{-1}$ , retaining about 51% of the value at the relatively low current density of  $1 \text{ A g}^{-1}$ .

**Table 1.** The capacitive performances of recently reported manganese oxide based materials.

Morphology	Synthesis route	Electrolyte salt	Capacitance ( $\text{F g}^{-1}$ )	Current density ( $\text{A g}^{-1}$ )	Cycle Numbers	Ref.
Nanowall array	Electrodeposition	0.1 M $\text{Na}_2\text{SO}_4$	327	1	1000	This paper
Nanosheet	Electrodeposition	1 M $\text{Na}_2\text{SO}_4$	201	1	3000	[9]
Nanosheet	Redox reaction	1 M $\text{Na}_2\text{SO}_4$	713.7	0.5	1200	[13]
Nanorod	Electrodeposition	0.5 M $\text{Na}_2\text{SO}_4$	362.5	0.5	5000	[14]
Spherical superstructure composed of thin nanoflakes	Hydrothermal method	3 M KOH	493	2	1000	[15]
Nanotube array	Electrodeposition	1 M $\text{Na}_2\text{SO}_4$	349	1	2000	[22]
Nanoporous film	hydrothermal method	6 M KOH	1086	5	500	[32]
nanosheet array	Electrodeposition	1 M $\text{Na}_2\text{SO}_4$	201	1	3000	[33]
Interconnected nanosheets	Electrodeposition	0.5 M $\text{Na}_2\text{SO}_4$	229	1	-	[34]
Nanowire array	Sol-gel template	2 M $(\text{NH}_4)_2\text{SO}_4$	165	$10 \text{ (mVs}^{-1}\text{)}$	-	[24] *
Nanowire arrays	Electrodeposition	0.5 M $\text{Na}_2\text{SO}_4$	254	$10 \text{ (mVs}^{-1}\text{)}$	-	[26] *
Nanowires	Electrodeposition	1 M $\text{Na}_2\text{SO}_4$	472	$10 \text{ (mVs}^{-1}\text{)}$	-	[28] *
macroporous film	Electrodeposition	0.5 M KCl	163.4	$10 \text{ (mVs}^{-1}\text{)}$	-	[29] *
Macroporous film	colloidal crystal-templating	5 M $\text{Na}_2\text{SO}_4$	765	$2 \text{ (mVs}^{-1}\text{)}$	2000	[31] *
Nanosheets	Electrodeposition	0.5 M $\text{Na}_2\text{SO}_4$	230	$20 \text{ (mVs}^{-1}\text{)}$	250	[36] *

\*Note: The specific capacitances from these researches were calculated from the CV curves at different scan rates.

Furthermore, the long cycle life stability of the nanostructured manganese oxide films was characterized by GCD cycling tests at  $1 \text{ A g}^{-1}$ . As shown in Fig. 4d, the SC value obtained from the oxide nanowall array reaches  $327 \text{ F g}^{-1}$  at the first cycle, and declines to a stable values of  $317 \text{ F g}^{-1}$  after the first 100 cycles. Then, the SC value remains stable in the following 1000 GCD cycles, retaining about 97 % of the initial values. The superior capacitance performance of the oxide nanowall

array can be attributed to their nanoporous microstructure which enhances the electrochemical utilization of manganese oxide during the redox reactions [17, 18]. As shown by Table 1, the manganese oxide nanowall array, compared with the recently reported manganese oxide based materials, can provide comparative better capacitive performances, proving to be a promising material for high performance supercapacitors.

#### 4. CONCLUSIONS

Nanostructured manganese oxide films, including continuous coating, nanoflower film and nanowall array, were successfully fabricated via a facile anodic electrodeposition technique. The nanowall array was composed of interconnected ultrathin nanosheets, of which the nanoporous microstructure can facilitate fast ions transportation and thus superior capacitive performances. As a result, the nanowall array exhibits superior capacitance performances. A high specific capacitance of  $327 \text{ F g}^{-1}$  is achieved at a GCD current density of  $1 \text{ A g}^{-1}$  for the nanowall array. The capacitance declines gradually to  $162 \text{ F g}^{-1}$  as the current density increased to  $15 \text{ A g}^{-1}$ , retaining about 51% of the value at the relatively low current density of  $1 \text{ A g}^{-1}$ . After 1000 GCD cycles, the nanowall array retained a high capacitance retention of 97%, indicating outstanding cycling performance as supercapacitor electrodes. Take into account of the facile and low cost fabrication process, the manganese oxide nanowall array could be a qualified candidate for the electrode material of supercapacitors.

#### ACKNOWLEDGEMENTS

This work was supported by National Natural Science Foundation of China (grant numbers U1504204 and 51774017).

#### References

1. G. Wang, L. Zhang and J. Zhang, *Chem. Soc. Rev.*, 41 (2012) 797.
2. Z.S. Iro, C. Subramani and S.S. Dash, *Int. J. Electrochem. Sci.*, 11 (2016) 10628.
3. L. Kouchachvili, W. Yaici and E. Entchev, *J. Power Sources*, 374 (2018) 237.
4. D.A.C. Brownson, D.K. Kampouris and C.E. Banks, *J. Power Sources*, 196 (2011) 4873.
5. S.J. Uke, V.P. Akhare, D.R. Bambole, A.B. Bodade and G.N. Chaudhari, *Front. Mater.*, 4 (2017).
6. C. Tanggarnjanavalukul, N. Phattharasupakun, K. Kongpatpanich and M. Sawangphruk, *Nanoscale*, 9 (2017) 13630.
7. K.S. Kumar, N. Choudhary, Y. Jung and J. Thomas, *ACS Energy Lett.*, 3 (2018) 482.
8. P. Simon and Y. Gogotsi, *Nat. Mater.*, 7 (2008) 845.
9. M. Kundu, L. Liu, *J. Power Sources*, 243 (2013) 676.
10. Z.P. Feng, G.R. Li, J.H. Zhong, Z.L. Wang, Y.N. Ou and Y.X. Tong, *Electrochem. Commun.*, 11 (2009) 706.
11. M. Huang, F. Li, F. Dong, Y.X. Zhang and L.L. Zhang, *J. Mater. Chem. A*, 3 (2015) 21380
12. D.D. Zheng, Y.J. Qiang, S.Y. Xu, W.P. Li, S.S. Yu and S.T. Zhang, *Appl. Phys. A-Mater. Sci. Process.*, 123 (2017).
13. W.H. Dang, C.J. Dong, Z.F. Zhang, G. Chen, Y.D. Wang and H.T. Guan, *Electrochim. Acta*, 217

- (2016) 16.
14. Z.G. Ye, T. Li, G. Ma, X.Y. Peng and J. Zhao, *J. Power Sources*, 351 (2017) 51.
  15. T. Zhu, Z.N. He, G.X. Zhang, Y.S. Lu, C. Lin, Y.G. Chen and H.B. Guo, *J. Alloy. Compd.*, 644 (2015) 186.
  16. Z.P. Ma, G.J. Shao, Y.Q. Fan, G.L. Wang, J.J. Song and D.J. Shen, *ACS Appl. Mater. Interfaces*, 8 (2016) 9050.
  17. J.W. Long, B. Dunn, D.R. Rolison and H.S. White, *Chem. Rev.* 104 (2004) 4463.
  18. C.-C. Hu, K.-H. Chang, M.-C. Lin and Y.-T. Wu, *Nano. Lett.* 6 (2006) 2690.
  19. S. Khalid, C.B. Cao, M. Naveed and W. Younas, *Sustain. Energ. Fuels*, 1 (2017) 1795.
  20. S.Y. Kong, K. Cheng, T. Ouyang, K. Ye, G.L. Wang, D.X. and Cao, *J. Electroanal. Chem.*, 786 (2017) 35.
  21. M. Huang, F. Li, F. Dong, Y.X. Zhang and L.L. Zhang, *J. Mater. Chem. A*, 3 (2015) 21380.
  22. H. Xia, J.K. Feng, H.L. Wang, M.O. Lai and L. Lu, *J. Power Sources*, 195 (2010) 4410.
  23. Z.W. Wei, Z., Z.X. Feng, L.X. Ze and J.N. Er, *J. Porous Mat.* 17 (2010) 253.
  24. X.Y. Wang, X.Y. Wang, W.G. Huang, P.J. Sebastian and S. Gamboa, *J. Power Sources*, 140 (2005) 211.
  25. H. Liu, B. Lu, S. Wei, M. Bao, Y. Wen and F. Wang, *Solid State Sci.* 14 (2012) 789.
  26. C.L. Xu, S.J. Bao, L.B. Kong, H. Li and H.L. Li, *J. Solid State Chem.* 179 (2006) 1351.
  27. A.L.M. Reddy, M.M. Shaijumon, S.R. Gowda and P.M. Ajayan, *J. Phys. Chem.* C114 (2010) 658.
  28. C.-L. Ho and M.-S. Wu, *J. Phys. Chem.* C115 (2011) 22068.
  29. M. Nakayama, T. Kanaya and R. Inoue, *Electrochem. Commun.* 9 (2007) 1154.
  30. T.M. Benedetti, V.R. Goncales, D.F.S. Petri, S.I.C. de Torresi and R.M. Torresi, *J. Brazil Chem. Soc.* 21 (2010) 1704.
  31. M. Sawangphruk and J. Limtrakul, *Mater. Lett.* 68 (2012) 230.
  32. Y.Y. Sun, W.H. Zhang, D.S. Li, L. Gao, C.L. and Hou, Y.H. Zhang and Y.Q. Liu, *Electrochim. Acta*, 178 (2015) 823.
  33. M. Kundu and L.F. Liu, *J. Power Sources*, 243 (2013) 676.
  34. W. Wei, X. Cui, X. Mao, W. Chen and D.G. Ivey, *Electrochim. Acta*, 56 (2011) 1619.
  35. D. Liu, Q. Zhang, P. Xiao, B.B. Garcia, Q. Guo, R. Champion and G. Cao, *Chem. Mater.* 20 (2008) 1376.
  36. B. Babakhani and D.G. Ivey, *J. Power Sources*, 196 (2011) 10762.
  37. Z.L. Huang, X. Zhao, J.L. Ren, J.X. Zhang, Y.Z. Li and Q.H. Zhang, *J. Nanosci. Nanotechnol.*, 16 (2016) 5668.
  38. W. Wei, X. Cui, W. Chen and D.G. Ivey, *J. Phys. Chem. C*, 112 (2008) 15075.
  39. T. Gao, P. Norby, F. Krumeich, H. Okamoto, R. Nesper and H. Fjellvåg, *J. Phys. Chem. C*, 114 (2010) 922.
  40. F. Ataherian, K.-T. Lee and N.-L. Wu, *Electrochim. Acta*, 55 (2010) 7429.
  41. J. Liu, J. Essner and J. Li, *Chem. Mater.*, 22 (2010) 5022.